Letter

Microwave signatures of topological superconductivity in planar Josephson junctions

Barış Pekerten,[1,*,†] David Brandão,[1,*,‡] Bassel Heiba Elfeky,[2] Tong Zhou,[1,3] Jong E. Han,[1] Javad Shabani,[2] and Igor Žutić[1,§]

[1]*Department of Physics, University at Buffalo, State University of New York, Buffalo, New York 14260, USA*
[2]*Center for Quantum Information Physics, Department of Physics, New York University, New York 10003, USA*
[3]*Eastern Institute for Advanced Study, Eastern Institute of Technology, Ningbo, Zhejiang 315200, China*

(Received 29 January 2024; revised 23 May 2024; accepted 22 July 2024; published 19 August 2024)

Planar Josephson junctions provide a platform to host topological superconductivity, which, through manipulating Majorana bound states (MBS), could enable fault-tolerant quantum computing. However, what constitutes experimental signatures of topological superconductivity and how MBS can be detected remains strongly debated. In addition to spurious effects that mimic MBS, there is a challenge to discern the inherent topological signals in realistic systems with many topologically trivial Andreev bound states, determining the transport properties of Josephson junctions. Guided by the advances in microwave spectroscopy, we theoretically study Al/InAs-based planar Josephson junction embedded into a radio-frequency superconducting quantum interference device to identify microwave signatures of topological superconductivity. Remarkably, by exploring the closing and reopening of a topological gap, we show that even in a wide planar Josephson junction with many Andreev bound states, such a topological signature is distinguishable in the resonance frequency shift of a microwave drive and the half-slope feature of the microwave absorption spectrum. Our findings provide an important step towards experimental detection of non-Abelian statistics and implementing scalable topological quantum computing.

DOI: 10.1103/PhysRevB.110.L060513

The interest in topological superconductors reflects their fascinating fundamental properties and potential applications using manipulation of Majorana bound states (MBS) [1–7]. However, detecting such topological superconductivity and MBS remains a long-standing challenge [8–11]. Revisiting Sr_2RuO_4, expected for decades to be p-wave spin-triplet, which could support MBS [12–15], or quantized zero-bias conductance peak (ZBCP) [16] as an experimental MBS signature [17] both provide cautionary guidance for various difficulties in detection of superconducting properties [10,18,19].

We focus on planar Josephson junctions (JJs) [20–27], where topological superconductivity is realized through proximity effects in the normal region (N) of two-dimensional electron gas (2DEG), which separates superconducting (S) regions, shown in Fig. 1(a). Such JJs, with a phase or gate control and multiterminal geometries suitable for probing non-Abelian statistics [28–30], could overcome limitations for topological superconductivity in 1D nanowires requiring fine-tuned parameters [7,31,32] and MBS detection through ZBCP.

Our approach builds on advances in circuit quantum electrodynamics and highly sensitive microwave spectroscopy of Andreev bound states (ABS) [33–37]. Due to electron-hole symmetry, ABS come in pairs and with energies $\pm E_{\mathrm{ABS}}(\phi)$, which depend on the relative superconducting phase, ϕ, between the two S regions. In contrast, MBS are topologically protected ABS with $E \approx 0$ localized to the ends of the junction that cannot be doubly occupied. To investigate these states, we theoretically consider an experimentally accurate model system where the planar JJ is embedded into a radio frequency superconducting quantum interference device (rf-SQUID), driven at a microwave frequency, f_d. The absorbed photons with $E = hf_d$ cause transitions between the ABS and change the JJ's critical current, I_c. By coupling the rf-SQUID to a microwave resonator, one can calculate this effect from the resulting change in the resonant frequency, f_r, of the resonator via a capacitively coupled transmission line [38–40], as shown in Fig. 1. This approach, using numerical discretization, allows us to calculate the ABS spectrum and topological phase diagram of the planar JJ, as well as the microwave spectra and the shift in the critical current.

Realistic planar JJs, in contrast with many microwave studies focusing on a few ABS, which is a characteristic for nanowires, atomic contacts, or constrictions, can have hundreds of topologically trivial ABS, which complicate detecting inherent properties of topological superconductivity and MBS [37,41–48]. Based on the experimental parameters of our fabricated JJs, we theoretically identify microwave signatures for closing and reopening of a topological gap. Our calculations show that such signatures are distinguishable in the transitions between the ABS due to a microwave drive of frequency, f_d, which change the current-phase relation (CPR), $I(\phi) = \Sigma_n I_n^{\mathrm{ABS}}$ that depends on the occupation of the

*These authors contributed equally to this work.
†Contact author: barispek@buffalo.edu
‡Contact author: dbrandao@buffalo.edu
§Contact author: zigor@buffalo.edu

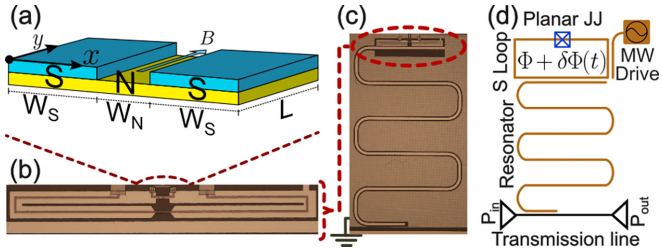

FIG. 1. (a) A planar JJ formed by two Al superconducting (S) regions covering InAs-based 2DEG normal region (N). Coordinate axes and JJ dimensions are indicated. Alternating current, I, flows along $\pm\hat{x}$; the applied magnetic field is $\boldsymbol{B}$. (b)–(d) Optical images of an example fabricated SQUID resonator, which we consider in our theoretical results. Gold: Al; dark brown: the etched mesa; and light brown: gate and a flux line. (c) Device diagram with resonator capacitively coupled to a transmission line and inductively to a superconducting loop with a flux Φ and a single JJ. (d) Schematic description from (c) of the JJ, SQUID, microwave drive line inducing fluctuations in $\Phi \to \Phi + \delta\Phi(t)$, resonator, and transmission line with input (output) power $P_{\rm in}$ ($P_{\rm out}$).

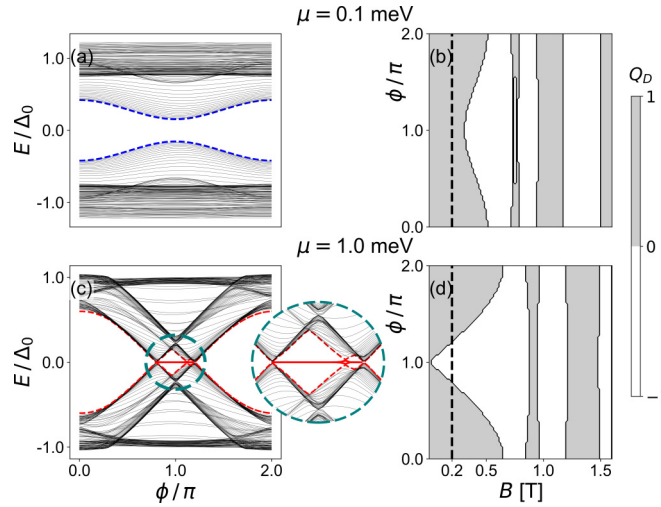

FIG. 2. (a), (c) ABS spectra as a function of ϕ for JJ from Fig. 1(a). $W_S = 600$ nm, $W_N = 80$ nm, $L = 4$ μm, and $B = 0.2$ T. (b), (d) The corresponding topological charge, Q_D, as a function of B and ϕ. (a), (b) For $\mu = 0.1$ meV, the gapped ABS are trivial for all ϕ. (c) For $\mu = 1.0$ meV, there is a gap closing and reopening. The inset: MBS at $E \approx 0$ (red solid line). (d) A topological transition as ϕ is varied at $B = 0.2$ T, corresponding to the gap closing points in (c).

ABS levels. This change in the CPR results in a shift in f_r, measured in the microwave circuit [38–40].

In microwave detection, a quality factor $\gtrsim$10000 and a linewidth of 0.1–1 MHz yield fast ($\sim\mu$s) and neV energy resolution of ABS [37,49]. In contrast to ZBCP measurements, this high sensitivity and fermion-parity conservation, which enables the probing of quasiparticle poisoning and dynamical properties of superconducting devices [40,49–51], make our findings important beyond signatures of topological superconductivity and MBS. These findings could also advance the microwave studies in many other systems with a large number of ABS, for example, in superconducting spintronics [8,52–54], in nonreciprocal phenomena such as diode effects [8,26,55–57], or in emerging superconducting qubits [58–60].

We consider a model Al/InAs-based JJ with $L = 4$ μm and $W_N = 80$ nm (see Fig. 1), embedded in an rf-SQUID, that is inductively coupled to a hanger $\lambda/4$ coplanar waveguide resonator for our calculations. The model resonator is capacitively coupled to a transmission feed line, allowing for the complex transmission and the resonant response to be measured. We use $f_r \sim 7$ GHz, estimated from experimentally relevant circuit parameters [38,39]. We therefore present our numerical results with f_d up to a few f_r (~40 GHz), unless showing the full range of $h\,f_d \lesssim 2\Delta_0 \sim 120$ GHz is instructive.

Our model for the microwave-driven JJ is described by the Bogoliubov-de Gennes (BdG) Hamiltonian [22,30]

$$H_0 = \left[\frac{\mathbf{p}^2}{2m^*} - \mu(x,y) + \frac{\alpha}{\hbar}(p_x\sigma_y - p_y\sigma_x)\right]\tau_z - \frac{g^*\mu_B}{2}\mathbf{B}\cdot\boldsymbol{\sigma} + \Delta(x,y)\tau_+ + \Delta^*(x,y)\tau_- , \quad (1)$$

for which numerically solve the corresponding discretized eigenvalue problem [61] to obtain ABS. Here, $\mathbf{p}$ is the momentum, $\mu(x,y)$ is the chemical potential, α is the Rashba spin-orbit coupling (SOC) strength, $\mathbf{B} = B\,\hat{y}$ is the in-plane magnetic field and μ_B is the Bohr magneton, while m^* and g^* are the effective mass and g factor, respectively. The proximity-induced superconductivity in the InAs 2DEG is described by the pair potential $\Delta(x,y) = \Delta_0\,\Theta(|x - W_N/2|)\,\exp[i\,\phi(x,y)/2]$, where Θ is the step function and in $\phi(x,y) = \phi_0\,\mathrm{sgn}(x)$, ϕ_0 is uniform in each S region. Similarly, we take $\Delta_0 \to \Delta_0(B,T)$ to be real and uniform in the S regions, having the usual BCS dependence on B and temperature T [30,62]. σ_i (τ_i) are Pauli (Nambu) matrices in the spin (particle-hole) space, and $\tau_\pm = (\tau_x \pm i\tau_y)/2$.

We choose material parameters consistent with our fabricated epitaxial Al/InAs JJs, which support robust proximity-induced superconductivity and topological transitions [26]: $\Delta_0 = 0.23$ meV, $m^* = 0.027m_0$ where m_0 is the electron mass, $g^* = 10$ for InAs, $\alpha = 10$ meV nm, critical magnetic field $B_c(T = 0) = 1.6$ T and temperature $T = 30$ mK. The corresponding ABS spectra are shown in Fig. 2. In the top row, for $\mu = 0.1$ meV and $B = 0.2$ T, the JJ is in the topologically trivial phase for all ϕ. In Fig. 2(a) there is no gap closing at $B = 0.2$ T, while in Fig. 2(b) the calculated topological charge [2], $Q_D = 1$, confirms this trivial phase. The mirror symmetry in the system with respect to the middle of the junction along the x direction allows for an effective time reversal symmetry, leading to a system that can support MBS in a wider range of ϕ values around $\phi = \pi$, as seen in Figs. 2(b) and 2(d) [22]. For a finite W_S, there are normal reflections and an imperfect transparency at the N/S interface, causing the topological phase diagram to deviate from the typical diamond shape [22,56,63] with a trivial phase even at $\phi = \pi$ and small B. In contrast, for a larger μ, the JJ in our model undergoes topological transitions even for $B \sim 0$ at $\phi = \pi$, leading to a wider range of ϕ that can support MBS for higher B [Fig. 2(d)]. At $B = 0.2$ T, MBS near $E \sim 0$ is seen in the spectrum in Fig. 2(c) and the inset for $0.8\pi < \phi < 1.2\pi$. In Supplemental Material (SM)

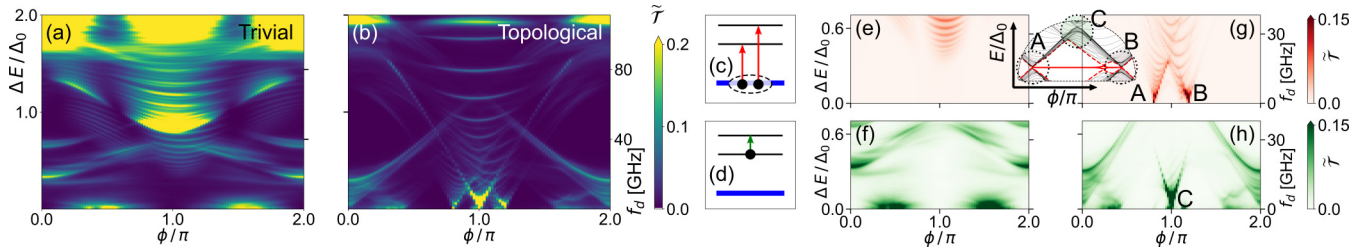

FIG. 3. (a), (b) Transition lines $\tilde{\mathcal{T}}(f,\phi)$, calculated using Eq. (4), corresponding to $hf_d = \Delta E = |E_n - E_m|$ between ABS from Figs. 2(a) and 2(c), with a Lorentzian broadening parameter $\epsilon = 30$ mK. In the schematic of (c) pair and (d) single-particle transitions where the ground state is denoted by a blue line, the sum of the arrow lengths in (c) gives ΔE. Resolving (e) pair and (f) single-particle transitions from (a) up to 40 GHz shows no gap closing and opening. In contrast a similarly resolved (g) pair and (h) single-particle transitions from (b) reveal signatures of topological superconductivity. The inset: an enlarged part of the Fig. 2(c) spectra. The transitions in the circles A and B of the inset lead to the V-shaped features A and B in (g), signaling a gap closing and reopening. Transitions in the circle C lead to the V-shaped feature C in (h).

[61], we complement these results with CPR, topological gap, the MBS localization, as well as topological phase transitions for larger μ as B is varied.

We next discuss the signatures of the topological gap closing and reopening in Fig. 2(c) using the microwave spectroscopy with the setup from Figs. 1(b)–1(d). The microwave drive induces a flux fluctuation, $\Phi(t) = \Phi(0) + \delta\Phi(t)$, in the rf-SQUID around its unperturbed value $\Phi(0)$, which leads to the JJ phase fluctuation $\delta\phi(t)$, described by the perturbed Hamiltonian [34,43,46,64–66]

$$H(\phi + \delta\phi(t)) = H_0(\phi) + \delta\phi(t)\, H_{\rm MW}, \tag{2}$$

where the perturbation $H_{\rm MW} = \partial H_0(\phi)\,/\,\partial\phi$ is given by

$$H_{\rm MW} = -i\,(\Delta_0/2)\,(e^{-i\phi(\mathbf{r})/2}\,\tau_+ - e^{i\phi(\mathbf{r})/2}\,\tau_-). \tag{3}$$

For our model experimental setup based on fabricated JJs embedded in microwave resonator circuits, we can examine the validity of this approach by a simple estimate, $\delta\phi/2\pi \sim M\,I_{\rm MW}/\Phi_0 < M\,I_c/\Phi_0 \approx 0.05$, where we use an experimentally relevant value of $M \sim 120$ pH for the mutual inductance and a critical current of $I_c \lesssim 1$ μA as an upper bound for the microwave driving current $I_{\rm MW}$ [67,68], thus justifying the treatment of the effects of the microwave drive as a perturbation [66,69,70]. The transitions caused by this perturbation conserve the fermion parity [43,51,61,66,71], which reduces the number of the allowed transition lines shown in Figs. 3(a) and 3(b). We can then distinguish the pair transitions, between a Cooper pair and two ABS, or the single-particle transitions between two ABS, as denoted in Figs. 3(c) and 3(d). In the BdG Hamiltonian, pair (single-particle) transitions correspond to transitions between the states with opposite (same) energy sign.

With high energy and time resolution, microwave spectroscopy provides information about the allowed transitions lines, $h\,f_d^{nm} = |E_m - E_n|$, with the transition probability $|\mathcal{M}_{nm}|^2$ governed by the matrix element $\mathcal{M}_{nm} = \langle\psi_m|H_{\rm MW}|\psi_n\rangle$, where ψ_n is the eigenstate with eigenenergy E_n of H_0 [Eq. (1)]. Our calculated results for planar JJs in Fig. 3 show the allowed transition lines

$$\mathcal{T}(f_d,\phi) = \sum_{mn} |\mathcal{M}_{nm}|^2 \mathcal{F}(E_m,E_n)\,\mathcal{L}(E_{mn} - hf_d), \tag{4}$$

where $\mathcal{F}(E_m,E_n)$ is the thermal occupation factor and $\mathcal{L}(E) = (\epsilon/\pi)/(E^2+\epsilon^2)$ the Lorentzian broadening, parameterized by ϵ. Figures 3(a) and 3(b), with the transition lines normalized to their maximum value, $\tilde{\mathcal{T}} = \mathcal{T}/\mathcal{T}_{\rm max}$, correspond to the system described by Figs. 2(a) and 2(c), respectively. While Fig. 3(a), which clearly shows the bulk band gap, as we see a very limited transition probability around $E \approx 0$ and $\phi \approx \pi$, we can conclude that Fig. 3(b) displays the gap closing signature of topological superconductivity.

Unlike the majority of the microwave studies with a much smaller number of ABS [37,43–46] with theoretical results that we can recover by reducing the system size of our model JJs [67,71,72], the several hundred ABS considered in Fig. 3 complicate the identification of topological superconductivity. To address this, we resolve the calculated transition lines into pair and single-particle transitions, now replotted up to $f_d = 40$ GHz, compatible with relevant experimental setups for microwave detection, instead of the full ABS energy range of $2\Delta_0$ or ∼120 GHz.

By comparing these two types of transitions for the trivial [Figs. 3(e) and 3(f)] and topological phase [Figs. 3(g) and 3(h)], we see some striking differences. This is further illustrated in the inset of Fig. 3(g), which is the enlarged version of Fig. 2(c) focusing on low-energy ABS spectra near the topological gap closing and reopening, and the matching features in Figs. 3(g) and 3(h). The features marked by A and B in the inset denote the locations of topological gap closing and reopening and the MBS at $E \approx 0$ between these points. The matching V-shaped features seen in Fig. 3(g), also marked by A and B, resolve the pair transition lines around the gap closing and reopening, which therefore mark the microwave signatures of the topological superconductivity. On the other hand, the V-shaped single-particle transition lines seen in Fig. 3(h), marked by C, correspond to the transitions between the ABS levels in a region far from $E \approx 0$ state (marked by C in the inset) and therefore are not related to topological superconductivity. We also note that the features near zero frequency at $\phi \sim \pi/2, 3\pi/2$ in Figs. 3(a), 3(b), 3(f), and 3(h) are related to single-particle transitions between ABS near $E \sim \Delta_0$, and are not topology related.

While, to the best of our knowledge, these here identified microwave signatures of topological superconductivity were not previously discussed, it is reassuring that for the trivial

phase, we recover the behavior known from the previous JJ studies. For example, by reducing the number of ABS that we consider, we retain all the main features of the previous work on the weak-link JJs [37]. This also includes the observed band gap around $\phi = \pi$ in Figs. 3(e) and 3(f), as expected for the trivial phase.

To provide further guidance to experimental work and previous $T = 0$ results for a small number of Andreev bound states [65,73,74], we consider the effects of the microwave drive on the JJ's CPR, which affects the f_r as discussed above. Without the microwave drive, the free energy of the JJ is $F = -k_B T \sum_{E_n} \ln[2\cosh(E_n/2k_BT)]$ [62], where k_B is the Boltzmann constant and $\{E_n\}$ is the spectrum for the JJ. The CPR, $I(\phi) = (2e/\hbar)\,\partial F / \partial\phi$, is then

$$I(\phi) = -\frac{e}{\hbar} \sum_{E_n} \frac{\partial E_n}{\partial \phi} \tanh\left(\frac{E_n}{2k_BT}\right). \tag{5}$$

Equation (5) shows the contribution of each energy level to the supercurrent, $(e/\hbar)\,\partial E_n/\partial\phi$, weighted by a thermal occupation $\tanh(E_n/2k_BT)$. We consider a change to $I(\phi)$ in Eq. (5) as a function of f_d, due to the microwave drive. At short timescales, we phenomenologically express the change in $I(\phi)$ as

$$\delta I(f,\phi) = \Gamma \sum_{m,n} \left(\frac{\partial E_m}{\partial \phi} - \frac{\partial E_n}{\partial \phi}\right) |\mathcal{M}_{mn}|^2 \times \mathcal{F}(E_m, E_n)\,\mathcal{L}(E_{mn} - hf_d). \tag{6}$$

We choose a special form of the thermal occupation $\mathcal{F}(E_m, E_n) = f_{\rm FD}(E_n)\,[1 - f_{\rm FD}(E_m)]$, where $f_{\rm FD}$ is the Fermi-Dirac function, to achieve the effect of suppressing single-particle transitions between the levels away from $E \approx 0$, due to the doubling of the fermionic degrees of freedom in the BdG Hamiltonian. This form of $\mathcal{F}(E_m, E_n)$ allows us to simulate the suppression of quasiparticle transitions between energy levels $E_{m,n}$ away from 0. The identification of topological signatures is simplified in the resulting transition lines $\widetilde{\mathcal{T}}$ and the shift in the current $\delta I(f,\phi)$. A counterpart plot with a conventional thermal occupation factor is discussed in SM [61]. In the limit of $T = 0$ K and $\epsilon = 0$, our Eq. (6) recovers the same form as in the published literature [65,73,74]. While Eq. (6) does not include the ϕ-dependent change of the slope and curvature of the ABS, our key results and trends are preserved by this simplification [38,61].

For the JJ from Fig. 2(c), with single-particle transitions where $|E| \gtrsim k_BT$, we use this approach to plot the transition lines in Figs. 4(a)–4(c) and $\delta I(f,\phi)$ of Eq. (6) in Figs. 4(d)–4(f). Both the transition lines and $\delta I(f,\phi)$ reveal the signatures of the gap closing and opening, even for a system with hundreds of ABS. While these low-frequency transitions near the gap closing points appear in Figs. 4(b) and 4(e) for the pair transition, an even more striking feature becomes visible in Figs. 4(c) and 4(f) for the single-particle transitions. The suppression of the higher-energy single-particle transitions, including the feature C in Fig. 3(h), removes the background that competes with the signal from transitions between the energy-split MBS and higher energies, now observed prominently in Fig. 4(c) as a transition line between $\phi \sim 0.8\pi$ and $\phi \sim 1.2\pi$ with half of the slope of the

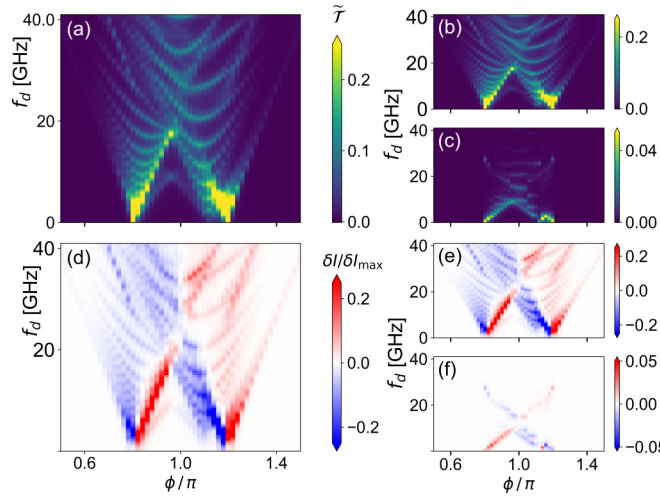

FIG. 4. (a)–(c) The transition lines and (d)–(f) $\delta I(f,\phi)$ for the ABS from Fig. 2(c) with suppressed higher-energy single-particle transitions. The lines $\widetilde{\mathcal{T}}(f,\phi)$ in (a) are resolved into (b) pair and (c) single-particle transitions. The remaining transition lines in (c) are due to the energy-split overlapping MBS. (d) $\delta I(f,\phi)$ displays the gap closing and reopening. $\delta I(f,\phi)$ shown from (e) pair and (f) single-particle transitions, reveals the gap closing and opening as well as the transitions from $E \approx 0$ split MBS.

V shapes marked by A and C in Fig. 3(g) [66,75]. This half-slope feature is also observed in Figs. 3–6 in the panels that depict topological transitions. The time-resolved capabilities of microwave spectroscopy could then also provide a detection of the non-Abelian statistics in planar JJs [29,30], which is supported by experimentally measured parameters, but is very challenging using conventional transport measurements.

Our overall features in Fig. 4 are consistent with other work on ABS in quantum dots [41,42], constrictions [43,44] and nanowires [37,45,46]. This is important for our effort to expand the microwave spectroscopy as a sensitive probe for topological superconductivity in systems with a large number of ABS, where additional signatures become more pronounced by resolving pair and single-particle transitions. For example, one could apply our proposed detection to topological JJs based on 2D materials [76], or systems with a

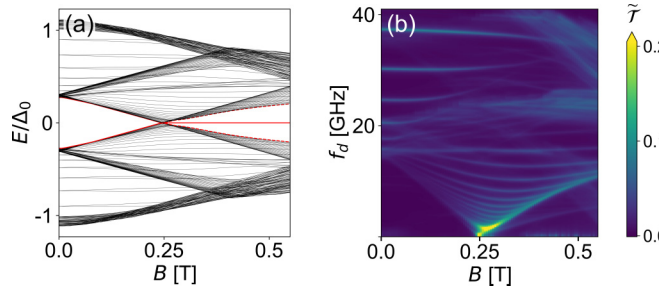

FIG. 5. (a) ABS spectrum as a function of B showing the lowest 240 levels with $\mu = 1$ meV and $\phi = 0.75\pi$. The gap closing and reopening, and the appearance of the zero-energy MBS at $B = 0.24$ T match the topological phase transition (see SM [61]). (b) Transition lines $\widetilde{\mathcal{T}}$ as a function of B. V feature indicating that the gap is closing and reopening is visible at $B = 0.24$ T near $f_d \sim 0$.

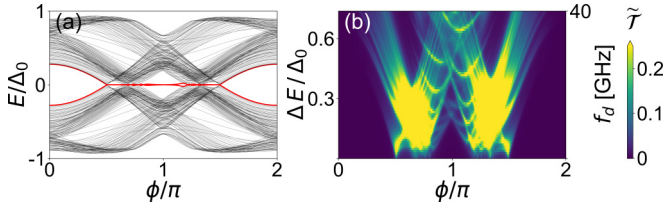

FIG. 6. (a) ABS spectrum as a function of ϕ showing the lowest 240 levels with $\mu = 5$ meV and $B = 0.5$ T, for $L = 4$ μm. (b) Transition lines $\widetilde{\mathcal{T}}$ as a function of B. The double-V feature, indicating the gap closing and reopening, is less sharp but visible around $\phi = 0.75\pi$ and $\phi = 1.25\pi$ near $f_d \sim 0$.

dominant cubic SOC where the topological superconductivity is expected to be f wave [77,78]. It would be interesting to test if the enhanced signatures, obtained by removing the single-particle transitions (violating fermion parity conservation), could be implemented experimentally by identification and dynamical selection of parity in JJs, demonstrated in atomic contacts [45,79] and weak links [69,80].

The V feature of topological gap closing and reopening is also seen in Fig. 5 from our numerical results for an experimental system where the JJ is phase biased and the Zeeman field is varied. We demonstrate the case where the phase bias is $\phi = 0.75\pi$ (at $\phi = \pi$ the transition would be very close to $B = 0$ T). The ABS spectrum in Fig. 5(a) and the topological phase diagram in SM [61] indicate a transition at $B = 0.24$ T. A corresponding V feature in the transition lines is observed in Fig. 5(b). The resolved pair transitions, and the $\delta I(f, B)$ plots in SM [61] also demonstrate the V feature and the gap reopening, indicating that topological transitions may be observed in phase-biased microwave experiments.

We next examine the influence of a higher chemical potential in a JJ with many ABS levels. The corresponding calculated results are shown in Fig. 6. By comparing the results for the spectra in Figs. 2(c) and 6(a), we see that at a higher μ will be less defined at a constant B as a function of ϕ, since a wider range of ABS levels will cross $E = 0$. This will result in a reduced topological gap and less protected MBS, and will lead to a less sharp V-shaped signature in the transition lines [Fig. 6(b)]. A larger B will shift the gap closing points further apart by shifting the ABS lines in the spectra, making the gap reopening signature more distinct. Similarly, a larger finite L will open the topological gap further, having the same effect of making the signatures more distinct (see SM [61]). In our simulations with $\mu = 5$ meV and $L = 4$ μm, $\alpha = 10$ meV nm at $B = 0.5$ T, the gap reopening signature remains prominently visible but less sharp in the transition lines.

Our findings have various implications beyond topological superconductivity. Microwave spectroscopy of ABS could provide a sensitive probe of nonreciprocal phenomena in JJs [8], while its temporal resolution could elucidate novel driving mechanism with time-dependent gate-control of SOC [81]. As a result, even in the absence of any bias current in the JJ, it is possible to consider enhanced opportunities for superconducting electronics and neuromorphic computing using voltage pulses corresponding to the single flux quantum [59,81–84]. With decades of transport studies in junctions with only a single superconductor [85], microwave detection also offers a complementary approach to revisit various manifestations of ABS and unconventional superconductivity.

Note added. Recently we were made aware of a publication [88] which is relevant to our work.

ACKNOWLEDGMENTS

We thank Prof. L. Glazman for valuable discussions. This work is supported by the U.S. ONR MURI Award No. N000142212764 and U.S. ONR Award No. N000141712793. Computational resources were provided by the UB Center for Computational Research.

[1] A. Kitaev, Fault-tolerant quantum computation by anyons, Ann. Phys. (NY) **303**, 2 (2003).
[2] C. Nayak, S. H. Simon, A. Stern, M. Freedman, and S. Das Sarma, Non-Abelian anyons and topological quantum computation, Rev. Mod. Phys. **80**, 1083 (2008).
[3] J. Alicea, Y. Oreg, G. Refael, F. von Oppen, and M. P. A. Fisher, Non-Abelian statistics and topological quantum information processing in 1D wire networks, Nat. Phys. **7**, 412 (2011).
[4] S. Das Sarma, M. Freedman, and C. Nayak, Majorana zero modes and topological quantum computation, npj Quant. Inf. **1**, 150001 (2015).
[5] A. Matos-Abiague, J. Shabani, A. D. Kent, G. L. Fatin, B. Scharf, and I. Žutić, Tunable magnetic textures: From Majorana bound states to braiding, Solid State Commun. **262**, 1 (2017).
[6] U. Güngördü and A. A. Kovalev, Majorana bound states with chiral magnetic textures, J. Appl. Phys. **132**, 041101 (2022).
[7] K. Laubscher and J. Klinovaja, Majorana bound states in semiconducting nanostructures, J. Appl. Phys. **130**, 081101 (2021).
[8] M. Amundsen, J. Linder, J. W. A. Robinson, I. Žutić, and N. Banerjee, Colloquium: Spin-orbit effects in superconducting hybrid structures, Rev. Mod. Phys. **96**, 021003 (2024).
[9] P. Yu, J. Chen, M. Gomanko, G. Badawy, E. P. A. M. Bakkers, K. Zuo, V. Mourik, and S. M. Frolov, Non-Majorana states yield nearly quantized conductance in proximatized nanowires, Nat. Phys. **17**, 482 (2021).
[10] J. Chen, B. D. Woods, P. Yu, M. Hocevar, D. Car, S. R. Plissard, E. P. A. M. Bakkers, T. D. Stanescu, and S. M. Frolov, Ubiquitous non-Majorana zero-bias conductance peaks in nanowire devices, Phys. Rev. Lett. **123**, 107703 (2019).
[11] E. J. H. Lee, X. Jiang, R. Aguado, G. Katsaros, C. M. Lieber, and S. De Franceschi, Zero-bias anomaly in a nanowire quantum dot coupled to superconductors, Phys. Rev. Lett. **109**, 186802 (2012).
[12] A. P. Mackenzie and Y. Maeno, The superconductivity of Sr_2RuO_4 and the physics of spin-triplet pairing, Rev. Mod. Phys. **75**, 657 (2003).
[13] T. M. Rice, Superfluid helium-3 has a metallic partner, Science **306**, 1142 (2004).

[14] K. D. Nelson, Z. Q. Mao, Y. Maeno, and Y. Liu, Odd-parity superconductivity in Sr_2RuO_4, Science **306**, 1151 (2004).

[15] S. Das Sarma, C. Nayak, and S. Tewari, Proposal to stabilize and detect half-quantum vortices in strontium ruthenate thin films: Non-Abelian braiding statistics of vortices in a $p_x + ip_y$ superconductor, Phys. Rev. B **73**, 220502(R) (2006).

[16] K. Sengupta, I. Žutić, H.-J. Kwon, V. M. Yakovenko, and S. Das Sarma, Midgap edge states and pairing symmetry of quasi-one-dimensional organic superconductors, Phys. Rev. B **63**, 144531 (2001).

[17] V. Mourik, K. Zuo, S. M. Frolov, S. R. Plissard, E. P. A. M. Bakkers, and L. P. Kouwenhoven, Signatures of Majorana fermions in hybrid superconductor-semiconductor nanowire devices, Science **336**, 1003 (2012).

[18] I. Žutić and I. Mazin, Phase-sensitive tests of the pairing state symmetry in Sr_2RuO_4, Phys. Rev. Lett. **95**, 217004 (2005).

[19] S. Das Sarma and H. Pan, Disorder-induced zero-bias peaks in Majorana nanowires, Phys. Rev. B **103**, 195158 (2021).

[20] J. Shabani, M. Kjaergaard, H. J. Suominen, Y. Kim, F. Nichele, K. Pakrouski, T. Stankevic, R. M. Lutchyn, P. Krogstrup, R. Feidenhans'l, S. Kraemer, C. Nayak, M. Troyer, C. M. Marcus, and C. J. Palmstrøm, Two-dimensional epitaxial superconductor-semiconductor heterostructures: A platform for topological superconducting networks, Phys. Rev. B **93**, 155402 (2016).

[21] M. Hell, M. Leijnse, and K. Flensberg, Two-dimensional platform for networks of Majorana bound states, Phys. Rev. Lett. **118**, 107701 (2017).

[22] F. Pientka, A. Keselman, E. Berg, A. Yacoby, A. Stern, and B. I. Halperin, Topological superconductivity in a planar Josephson junction, Phys. Rev. X **7**, 021032 (2017).

[23] A. Fornieri, A. M. Whiticar, F. Setiawan, E. Portolés, A. C. C. Drachmann, A. Keselman, S. Gronin, C. Thomas, T. Wang, R. Kallaher, G. C. Gardner, E. Berg, M. J. Manfra, A. Stern, C. M. Marcus, and F. Nichele, Evidence of topological superconductivity in planar Josephson junctions, Nature (London) **569**, 89 (2019).

[24] H. Ren, F. Pientka, S. Hart, A. Pierce, M. Kosowsky, L. Lunczer, R. Schlereth, B. Scharf, E. M. Hankiewicz, L. W. Molenkamp, B. I. Halperin, and A. Yacoby, Topological superconductivity in a phase-controlled Josephson junction, Nature (London) **569**, 93 (2019).

[25] F. Setiawan, C.-T. Wu, and K. Levin, Full proximity treatment of topological superconductors in Josephson-junction architectures, Phys. Rev. B **99**, 174511 (2019).

[26] M. C. Dartiailh, W. Mayer, J. Yuan, K. S. Wickramasinghe, A. Matos-Abiague, I. Žutić, and J. Shabani, Phase signature of topological transition in Josephson junctions, Phys. Rev. Lett. **126**, 036802 (2021).

[27] A. Banerjee, O. Lesser, M. A. Rahman, H.-R. Wang, M.-R. Li, A. Kringhøj, A. M. Whiticar, A. C. C. Drachmann, C. Thomas, T. Wang, M. J. Manfra, E. Berg, Y. Oreg, A. Stern, and C. M. Marcus, Signatures of a topological phase transition in a planar Josephson junction, Phys. Rev. B **107**, 245304 (2023).

[28] L. Fu and C. L. Kane, Superconducting proximity effect and Majorana fermions at the surface of a topological insulator, Phys. Rev. Lett. **100**, 096407 (2008).

[29] T. Zhou, M. C. Dartiailh, W. Mayer, J. E. Han, A. Matos-Abiague, J. Shabani, and I. Žutić, Phase control of Majorana bound states in a topological X junction, Phys. Rev. Lett. **124**, 137001 (2020).

[30] T. Zhou, M. C. Dartiailh, K. Sardashti, J. E. Han, A. Matos-Abiague, J. Shabani, and I. Žutić, Fusion of Majorana bound states with mini-gate control in two-dimensional systems, Nat. Commun. **13**, 1738 (2022).

[31] R. M. Lutchyn, J. D. Sau, and S. Das Sarma, Majorana fermions and a topological phase transition in semiconductor-superconductor heterostructures, Phys. Rev. Lett. **105**, 077001 (2010).

[32] Y. Oreg, G. Refael, and F. von Oppen, Helical liquids and majorana bound states in quantum wires, Phys. Rev. Lett. **105**, 177002 (2010).

[33] N. M. Chtchelkatchev and Y. V. Nazarov, Andreev quantum dots for spin manipulation, Phys. Rev. Lett. **90**, 226806 (2003).

[34] M. A. Despósito and A. L. Yeyati, Controlled dephasing of Andreev states in superconducting quantum point contacts, Phys. Rev. B **64**, 140511(R) (2001).

[35] L. Bretheau, C. O. Girit, H. Pothier, D. Esteve, and C. Urbina, Exciting Andreev pairs in a superconducting atomic contact, Nature (London) **499**, 312 (2013).

[36] A. A. Reynoso, G. Usaj, C. A. Balseiro, D. Feinberg, and M. Avignon, Spin-orbit-induced chirality of Andreev states in Josephson junctions, Phys. Rev. B **86**, 214519 (2012).

[37] L. Tosi, C. Metzger, M. F. Goffman, C. Urbina, H. Pothier, S. Park, A. L. Yeyati, J. Nygård, and P. Krogstrup, Spin-orbit splitting of Andreev states revealed by microwave spectroscopy, Phys. Rev. X **9**, 011010 (2019).

[38] S. Park, C. Metzger, L. Tosi, M. F. Goffman, C. Urbina, H. Pothier, and A. L. Yeyati, From adiabatic to dispersive readout of quantum circuits, Phys. Rev. Lett. **125**, 077701 (2020).

[39] D. M. Pozar, *Microwave Engineering*, 4th ed. (Wiley, Hoboken, 2012).

[40] B. H. Elfeky, W. M. Strickland, J. Lee, J. T. Farmer, S. Shanto, A. Zarassi, D. Langone, M. G. Vavilov, E. M. Levenson-Falk, and J. Shabani, Quasiparticle dynamics in epitaxial Al-InAs planar Josephson junctions, PRX Quantum **4**, 030339 (2023).

[41] R. S. Deacon, Y. Tanaka, A. Oiwa, R. Sakano, K. Yoshida, K. Shibata, K. Hirakawa, and S. Tarucha, Tunneling spectroscopy of Andreev energy levels in a quantum dot coupled to a superconductor, Phys. Rev. Lett. **104**, 076805 (2010).

[42] P. Zhang, H. Wu, J. Chen, S. A. Khan, P. Krogstrup, D. Pekker, and S. M. Frolov, Signatures of Andreev blockade in a double quantum dot coupled to a superconductor, Phys. Rev. Lett. **128**, 046801 (2022).

[43] C. Janvier, L. Tosi, L. Bretheau, C. O. Girit, M. Stern, P. Bertet, P. Joyez, D. Vion, D. Esteve, M. F. Goffman, H. Pothier, and C. Urbina, Coherent manipulation of Andreev states in superconducting atomic contacts, Science **349**, 1199 (2015).

[44] A. Wallraff, D. I. Schuster, A. Blais, L. Frunzio, R.-S. Huang, J. Majer, S. Kumar, S. M. Girvin, and R. J. Schoelkopf, Strong coupling of a single photon to a superconducting qubit using circuit quantum electrodynamics, Nature (London) **431**, 162 (2004).

[45] D. J. van Woerkom, A. Proutski, B. van Heck, D. Bouman, J. I. Väyrynen, L. I. Glazman, P. Krogstrup, J. Nygård, L. P. Kouwenhoven, and A. Geresdi, Microwave spectroscopy of spinful Andreev bound states in ballistic semiconductor Josephson junctions, Nat. Phys. **13**, 876 (2017).

[46] M. Hays, V. Fatemi, D. Bouman, J. Cerrillo, S. Diamond, K. Serniak, T. Connolly, P. Krogstrup, J. Nygård, A. L. Yeyati, A. Geresdi, and M. H. Devoret, Coherent manipulation of an Andreev spin qubit, Science **373**, 430 (2021).

[47] D. Pekker, C.-Y. Hou, V. E. Manucharyan, and E. Demler, Proposal for coherent coupling of Majorana zero modes and superconducting qubits using the 4π Josephson effect, Phys. Rev. Lett. **111**, 107007 (2013).

[48] F. J. Matute-Cañadas, C. Metzger, S. Park, L. Tosi, P. Krogstrup, J. Nygård, M. F. Goffman, C. Urbina, H. Pothier, and A. L. Yeyati, Signatures of interactions in the Andreev spectrum of nanowire Josephson junctions, Phys. Rev. Lett. **128**, 197702 (2022).

[49] M. Hays, G. de Lange, K. Serniak, D. J. van Woerkom, D. Bouman, P. Krogstrup, J. Nygård, A. Geresdi, and M. H. Devoret, Direct microwave measurement of Andreev-bound-state dynamics in a semiconductor-nanowire Josephson junction, Phys. Rev. Lett. **121**, 047001 (2018).

[50] V. D. Kurilovich, C. Murthy, P. D. Kurilovich, B. van Heck, L. I. Glazman, and C. Nayak, Quantum critical dynamics of a Josephson junction at the topological transition, Phys. Rev. B **104**, 014509 (2021).

[51] F. Kos, S. E. Nigg, and L. I. Glazman, Frequency-dependent admittance of a short superconducting weak link, Phys. Rev. B **87**, 174521 (2013).

[52] J. Linder and J. W. A. Robinson, Superconducting spintronics, Nat. Phys. **11**, 307 (2015).

[53] M. Eschrig, Spin-polarized supercurrents for spintronics: A review of current progress, Rep. Prog. Phys. **78**, 104501 (2015).

[54] R. Cai, I. Žutić, and W. Han, Superconductor/ferromagnet heterostructures: A platform for superconducting spintronics and quantum computation, Adv. Quantum Technol. **6**, 2200080 (2023).

[55] C. Baumgartner, L. Fuchs, A. Costa, S. Reinhardt, S. Gronin, G. C. Gardner, T. Lindemann, M. J. Manfra, P. E. F. Junior, D. Kochan, J. Fabian, N. Paradiso, and C. Strunk, Supercurrent rectification and magnetochiral effects in symmetric Josephson junctions, Nat. Nanotechnol. **17**, 39 (2022).

[56] B. Pekerten, J. D. Pakizer, B. Hawn, and A. Matos-Abiague, Anisotropic topological superconductivity in Josephson junctions, Phys. Rev. B **105**, 054504 (2022).

[57] N. Lotfizadeh, W. F. Schiela, B. Pekerten, P. Yu, W. Strickland, A. Matos-Abiague, and J. Shabani, Superconducting diode effect sign change in epitaxial Al-InAs Josepshon junctions, Commun. Phys. **7**, 120 (2024).

[58] P. Krantz, M. Kjaergaard, F. Yan, T. P. Orlando, S. Gustavsson, and W. D. Oliver, A quantum engineer's guide to superconducting qubits, Appl. Phys. Rev. **6**, 021318 (2019).

[59] F. Tafuri (ed.), *Fundamentals and Frontiers of the Josephson Effect* (Springer Nature, Cham, 2019).

[60] M. Pita-Vidal, A. Bargerbos, C.-K. Yang, D. J. van Woerkom, W. Pfaff, N. Haider, P. Krogstrup, L. P. Kouwenhoven, G. de Lange, and A. Kou, Gate-tunable field-compatible fluxonium, Phys. Rev. Appl. **14**, 064038 (2020).

[61] See Supplemental Material at http://link.aps.org/supplemental/10.1103/PhysRevB.110.L060513 for the details of the numerical calculations, as well as further discussions on the current-phase relationship, quasiparticle poisoning, MW perturbation of the critical current, topological transitions through changing Zeeman field, and higher chemical potential results, which includes Refs. [2,22,26,40,56,86,87].

[62] M. Tinkham, *Introduction to Superconductivity* (McGraw-Hill, New York, 1996).

[63] B. Pekerten, D. S. Brandão, B. Bussiere, D. Monroe, T. Zhou, J. E. Han, J. Shabani, A. Matos-Abiague, and I. Žutić, Beyond the standard model of topological Josephson junctions: From crystalline anisotropy to finite-size and diode effects, Appl. Phys. Lett. **124**, 252602 (2024).

[64] A. Zazunov, V. S. Shumeiko, E. N. Bratus', J. Lantz, and G. Wendin, Andreev level qubit, Phys. Rev. Lett. **90**, 087003 (2003).

[65] D. G. Olivares, A. L. Yeyati, L. Bretheau, C. O. Girit, H. Pothier, and C. Urbina, Dynamics of quasiparticle trapping in Andreev levels, Phys. Rev. B **89**, 104504 (2014).

[66] J. I. Väyrynen, G. Rastelli, W. Belzig, and L. I. Glazman, Microwave signatures of Majorana states in a topological Josephson junction, Phys. Rev. B **92**, 134508 (2015).

[67] M. C. Dartiailh, J. J. Cuozzo, B. H. Elfeky, W. Mayer, J. Yuan, K. S. Wickramasinghe, E. Rossi, and J. Shabani, Missing Shapiro steps in topologically trivial Josephson junction on InAs quantum well, Nat. Commun. **12**, 78 (2021).

[68] D. Phan, P. Falthansl-Scheinecker, U. Mishra, W.M. Strickland, D. Langone, J. Shabani, and A.P. Higginbotham, Gate-tunable superconductor-semiconductor parametric amplifier, Phys. Rev. Appl. **19**, 064032 (2023).

[69] J. J. Wesdorp, F. J. Matute-Cañadas, A. Vaartjes, L. Grünhaupt, T. Laeven, S. Roelofs, L. J. Splitthoff, M. Pita-Vidal, A. Bargerbos, D. J. van Woerkom, P. Krogstrup, L. P. Kouwenhoven, C. K. Andersen, A. L. Yeyati, B. van Heck, and G. de Lange, Microwave spectroscopy of interacting Andreev spins, Phys. Rev. B **109**, 045302 (2024).

[70] V. Chidambaram, A. Kringhoj, L. Casparis, F. Kuemmeth, T. Wang, C. Thomas, S. Gronin, G. C. Gardner, Z. Cui, C. Liu, K. Moors, M. J. Manfra, K. D. Petersson, and M. R. Connolly, Microwave sensing of Andreev bound states in a gate-defined superconducting quantum point contact, Phys. Rev. Res. **4**, 023170 (2022).

[71] L. Bretheau, J.I.-J. Wang, R. Pisoni, K. Watanabe, T. Taniguchi, and P. Jarillo-Herrero, Tunnelling spectroscopy of Andreev states in graphene, Nat. Phys. **13**, 756 (2017).

[72] B. H. Elfeky, J. J. Cuozzo, N. Lotfizadeh, W. F. Schiela, S. M. Farzaneh, W. M. Strickland, D. Langone, E. Rossi, and J. Shabani, Evolution of 4π-periodic supercurrent in the presence of an in-plane magnetic field, ACS Nano **17**, 4650 (2023).

[73] A. Blais, A. L. Grimsmo, S. M. Girvin, and A. Wallraff, Circuit quantum electrodynamics, Rev. Mod. Phys. **93**, 025005 (2021).

[74] L. Bretheau, C. O. Girit, M. Houzet, H. Pothier, D. Esteve, and C. Urbina, Theory of microwave spectroscopy of Andreev bound states with a Josephson junction, Phys. Rev. B **90**, 134506 (2014).

[75] C. Murthy, V. D. Kurilovich, P. D. Kurilovich, B. van Heck, L. I. Glazman, and C. Nayak, Energy spectrum and current-phase relation of a nanowire Josephson junction close to the topological transition, Phys. Rev. B **101**, 224501 (2020).

[76] Y.-M. Xie, É. Lantagne-Hurtubise, A. F. Young, S. Nadj-Perge, and J. Alicea, Gate-defined topological Josephson junctions in Bernal bilayer graphene, Phys. Rev. Lett. **131**, 146601 (2023).

[77] M. Alidoust, C. Shen, and I. Žutić, Cubic spin-orbit coupling and anomalous Josephson effect in planar junctions, Phys. Rev. B **103**, L060503 (2021).

[78] M. Luethi, K. Laubscher, S. Bosco, D. Loss, and J. Klinovaja, Planar Josephson junctions in germanium: Effect of cubic spin-orbit interaction, Phys. Rev. B **107**, 035435 (2023).

[79] L. Bretheau, C. O. Girit, C. Urbina, D. Esteve, and H. Pothier, Supercurrent spectroscopy of Andreev states, Phys. Rev. X **3**, 041034 (2013).

[80] N. Ackermann, A. Zazunov, S. Park, R. Egger, and A. L. Yeyati, Dynamical parity selection in superconducting weak links, Phys. Rev. B **107**, 214515 (2023).

[81] D. Monroe, M. Alidoust, and I. Žutić, Tunable planar Josephson junctions driven by time-dependent spin-orbit coupling, Phys. Rev. Appl. **18**, L031001 (2022).

[82] D. S. Holmes, A. L. Ripple, and M. A. Manheimer, Energy-efficient superconducting computing-power budgets and requirements, IEEE Trans. Appl. Supercond. **23**, 1701610 (2013).

[83] K. K. Likharev and V. K. Semenov, RSFQ logic/memory family: A new Josephson-junction technology for sub-terahertz-clock-frequency digital systems, IEEE Trans. Appl. Supercond. **1**, 3 (1991).

[84] P. Crotty, D. Schult, and K. Segall, Josephson junction simulation of neurons, Phys. Rev. E **82**, 011914 (2010).

[85] S. Kashiwaya and Y. Tanaka, Tunnelling effects on surface bound states in unconventional superconductors, Rep. Prog. Phys. **63**, 1641 (2000).

[86] C. W. Groth, A. R. Akhmerov, and X. Waintal, Kwant: a software package for quantum transport, New J. Phys. **16**, 063065 (2014).

[87] S. Tewari and J. D. Sau, Topological invariants for spin-orbit coupled superconductor nanowires, Phys. Rev. Lett. **109**, 150408 (2012).

[88] M. Trif, O. Dmytruk, H. Bouchiat, R. Aguado, and P. Simon, Dynamic current susceptibility as a probe of Majorana bound states in nanowire-based Josephson junctions, Phys. Rev. B **97**, 041415 (2018).